

## STUDIES OF REACTION DYNAMICS IN THE FERMI ENERGY DOMAIN

M. VESELSKY, G.A. SOULIOTIS, S.J. YENNELLO

*Cyclotron Institute, Texas A&M University, College Station TX 77843, USA  
E-mail: veselsky@comp.tamu.edu*

An overview of recent results on reaction dynamics in the energy region 20 - 50 A.MeV is given. The results of the study of projectile multifragmentation using the detector array FAUST are presented. Reaction mechanism is determined and thermodynamical properties of the hot quasiprojectile are investigated. Preliminary results on fragment isospin asymmetry obtained using the  $4\pi$  detector array NIMROD are given. Procedure for selecting centrality in two-dimensional multiplicity histograms is described. Possibility to extract thermodynamical temperature from systematics of isotope ratios is investigated. Reaction mechanism leading to production of hot sources is discussed. Furthermore, the possibilities for production of rare isotopes are discussed and recent experimental results obtained using recoil separator MARS are presented.

### 1 Introduction

Nucleus-nucleus collisions in the Fermi energy domain ( projectile energies 20 - 100 A MeV ) exhibit large variety of possible scenarios. In very peripheral collisions the relative motion of the projectile and target nuclei is mostly tangential and only few nucleons are exchanged in the region close to the contact of the surfaces. In more damped peripheral collisions nuclei still preserve their identity and a di-nuclear system is created due to friction forces. In such cases a considerable amount of nucleons can be exchanged and hot nuclei can be formed. With further decrease of the impact parameter, the energy of the radial motion increases and violent scenarios can take place where essential parts of both nuclei join into one hot nucleus. Hot nuclei created in both peripheral and central collisions can undergo multifragmentation. The process of multifragmentation is of interest for studies of thermodynamic properties of nuclear systems. Experimental studies of multifragmentation require multidetector systems with large geometric coverage. An essential information about the hot system can be collected using such devices and detailed studies can be carried out. In this proceeding we present results of multifragmentation studies using the forward array FAUST and the  $4\pi$  detector array NIMROD. Properties of the hot emitting source are investigated. From the practical point of view, reactions in the Fermi energy domain can provide a new approach to production of rare beams. In particular the projectile-like nuclei are

of interest for the production of rare isotopes because of the extensive nucleon exchange. We present here the results of studies of  $^{86}\text{Kr}$  fragmentation at 25 A MeV using recoil separator MARS along with comparison to results of model calculations.

## 2 Projectile multifragmentation

Projectile fragmentation has traditionally been thought of as a two-step reaction with excitation via a peripheral collision with the target followed by fragmentation of the projectile. In this framework, the influence of the mass and charge of the target nucleus on projectile fragmentation is a question of interest both with regard to formation of the excited quasiprojectile and its subsequent fragmentation. A cycle of works <sup>1,2,3,4</sup> on projectile multifragmentation of a  $^{28}\text{Si}$  beam in the reaction with  $^{112}\text{Sn}$  and  $^{124}\text{Sn}$  targets at 30 and 50 A MeV was carried out recently at the Cyclotron Institute of Texas A&M University.

The experiment was done with a beam of  $^{28}\text{Si}$  impinging on  $\sim 1$  mg/cm<sup>2</sup> self supporting  $^{112,124}\text{Sn}$  targets. The beam was delivered at 30 and 50 A MeV by the K500 superconducting cyclotron at the Cyclotron Institute of Texas A&M University. The detector array FAUST <sup>5</sup> consisting of 68 silicon - CsI(Tl) telescopes covering polar angles from 2.3° to 33.6° in the laboratory system was used. The detectors are arranged in five concentric rings. The geometrical efficiency is approximately 90% for the angle range covered. Isotopes of light charged particles and intermediate-mass fragments up to a charge of  $Z_f = 5$  were identified. Additional particle telescopes at angles between 42.5-82.5° and 123-147° complemented the forward array in the setup. Details of the experimental procedure and detector calibration can be found in ref. <sup>1</sup>.

The study <sup>2</sup> was restricted to events where all emitted fragments were isotopically identified (  $Z_f < 5$  ). We assumed that such events detected in the FAUST detector array originate predominantly from the deexcitation of the quasiprojectile ( or projectile-like source ). This assumption was supported by the Gaussian shape of the quasiprojectile velocity distributions and by low multiplicities of coincident charged particles at backward angles <sup>2</sup>. Considerable asymmetry of the projectile-target system leads already in peripheral collisions to production of highly excited light quasiprojectiles while the target nucleus remains much colder and de-excites mostly via emission of neutrons. The influence of pre-equilibrium emission was found <sup>2</sup> to be weak and could not influence the reaction scenario dramatically. The total charge of the reconstructed quasiprojectile ( QP ) was restricted to the values near

the projectile charge ( $Z_{QP} = 12 - 15$ ). This very selective data contains information on fragmentation of highly excited projectile-like prefragments, and thus can be used to study the mechanism of dissipation of the kinetic energy of relative motion into thermal degrees of freedom.

Useful experimental information about the nucleon exchange rate can be found in the events where the charge of the reconstructed quasiprojectile is equal to the charge of incident beam ( $Z_{QP} = 14$ ). In this case, isospin equilibration may only occur by the transfer of neutrons, as the number of transferred neutrons is the only available isospin degree of freedom of the system. Since the neutron number of the reconstructed quasiprojectile is just a sum of neutrons bound in the fragments with non-zero charge, we defined a principal neutron exchange observable as the mass change. Subtracting the sum of the neutrons bound in the detected fragments from the neutron number of the beam gives

$$\Delta A = N_{proj} - \sum_f N_f \quad (1)$$

where  $N_{proj} = 14$  for  $^{28}\text{Si}$  beam.

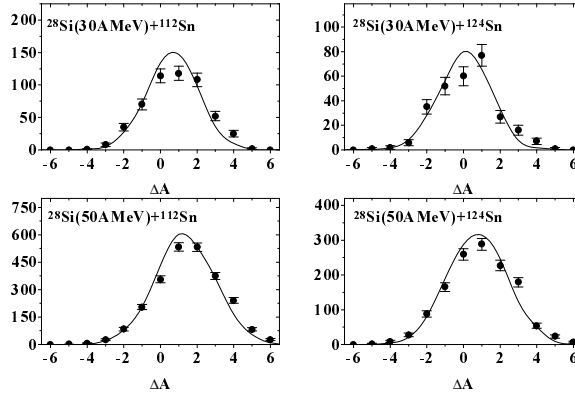


Figure 1. Experimental (solid circles) and simulated (solid lines) mass change distributions for the fully isotopically resolved quasiprojectiles with  $Z_{QP} = 14$  <sup>2</sup>.

Experimental mass change distributions for both projectile energies and target isotopes are shown in Fig. 1 as circles. When looking at the shapes of the observed  $\Delta A$  distributions, it is apparent that they are almost identical for different targets at the same projectile energy and are close to Gaussians.

For both projectile energies the mean value of the mass change is larger for the reaction with the  $^{112}\text{Sn}$  target by a little more than half a unit ( 0.60 for 30 A MeV and 0.65 for 50 A MeV ). The experimental distributions of the mass change are compared to simulated ones for fully isotopically resolved events with  $Z_{QP} = 14$  ( solid lines ). The basic assumption of the simulation is the possibility to decompose the collision into two stages. In the early stage of the collision hot quasiprojectiles are created which then deexcite by the statistical decay. To describe the production of excited quasiprojectiles we used the Monte Carlo code of Tassan-Got et al. <sup>6</sup>. This code implements a version of the model of deep inelastic transfer suitable for Monte Carlo simulations. De-excitation of the highly excited quasiprojectile was simulated using the statistical model of multifragmentation ( SMM ) <sup>7</sup>. Macrocanonical partitions of fragments were generated for individual events. The agreement of the experimental and simulated distributions of the mass change is reasonable. This implies that both the nucleon exchange and de-excitation are described adequately. To further justify such a conclusion, an apparent charged particle excitation energy of the quasiprojectile was reconstructed for each projectile fragmentation event from the energy balance in the center of mass frame of the quasiprojectile. Thus

$$E_{app}^* = \sum_f (T_f^{QP} + \Delta m_f) - \Delta m_{QP} , \quad (2)$$

where  $T_f^{QP}$  is the kinetic energy of the fragment in the reference frame of the quasiprojectile and  $\Delta m_f$  and  $\Delta m_{QP}$  are the mass excesses of the fragment and quasiprojectile, respectively.

The distributions of apparent quasiprojectile excitation energies reconstructed from fully isotopically resolved events are shown in Fig. 2. The reconstructed distributions for multifragmentation events with  $Z_{QP} = 14$  are represented as circles. Squares represent a broader set of events with  $Z_{QP} = 12 - 15$ . In Fig. 2 are also shown the simulated distributions of apparent quasiprojectile excitation energies for both  $Z_{QP} = 14$  and  $Z_{QP} = 12 - 15$  ( solid histograms ). The simulated data have been normalized to the sum of experimental events with  $Z_{QP} = 12 - 15$ . The agreement of the simulated and experimental apparent quasiprojectile excitation energy distributions with both  $Z_{QP} = 12 - 15$  and  $Z_{QP} = 14$  is quite good. The onset of multifragmentation into channels with  $Z_f \leq 5$  in the low energy part is described with good precision for both sets of data  $Z_{QP} = 12 - 15$  and  $Z_{QP} = 14$ .

The set of data obtained here allows further study of thermal quasiprojectile multifragmentation, especially the study of influence of the quasiprojectile

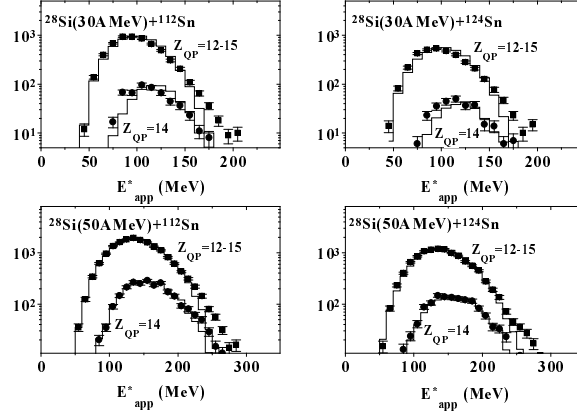


Figure 2. Distributions of apparent excitation energies of the quasiprojectiles. Symbols mean experimental distributions of the set of isotopically resolved quasiprojectiles with  $Z_{QP} = 14$  ( solid circles ) and  $Z_{QP} = 12 - 15$  ( solid squares )<sup>2</sup>. Solid histograms mean simulated distributions.

isospin asymmetry on properties of the fragmenting system. This data is of specific interest because the isospin asymmetry of the system which actually undergoes multifragmentation is known with good precision. Fig. 3 shows dependences of the isobaric yield ratio  $Y(^3\text{H})/Y(^3\text{He})$  on  $N/Z_{QP}$  for nine bins of the apparent excitation energy per mass unit of the quasiprojectile ( $\epsilon_{app}^*$ ). The data for both targets and projectile energies were combined to increase the statistics. This is possible because for a given excitation energy bin, the  $Y(^3\text{H})/Y(^3\text{He})$  dependences agree within the statistical deviations. The experimental data are represented as squares and the lines show the fits. As one can see on Fig. 3, linearity is the overall feature of the logarithmic plots of the  $Y(^3\text{H})/Y(^3\text{He})$  ratio in all excitation energy bins and is especially significant in the excitation energy bins with high statistics. The slopes are steepest at low excitation energies and become flatter with increasing excitation energy.

Within the approximation described in detail in<sup>4</sup>, the expression for the isobaric ratio  $Y(^3\text{H})/Y(^3\text{He})$  will be

$$\ln(Y(^3\text{H})/Y(^3\text{He})) = \ln(K(T)) + (\mu_n - \mu_p)/T \quad (3)$$

where  $K(T)$  is a proportionality factor dependent on the temperature but independent of the  $N/Z$  ratio of the fragmenting system. The difference of chemical potentials for neutrons and protons  $\mu_n - \mu_p$  was approximated by

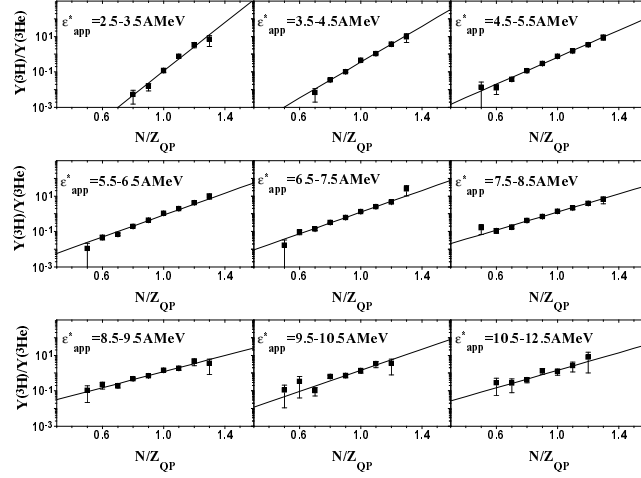


Figure 3. Dependence of the yield ratio  $Y(^3\text{H})/Y(^3\text{He})$  on  $N/Z$  ratio of the isotopically resolved quasiprojectiles with  $Z_{QP} = 12 - 15$  for nine bins of  $\epsilon_{app}^*$ .<sup>4</sup>

the difference of proton and neutron separation energies in the ground state  $S_p - S_n$ . Experimental mass excesses<sup>8</sup> have been used for the evaluation. The dependence of  $S_p - S_n$  on the  $N/Z$  ratio of the quasiprojectile can be considered linear with good precision. Formula 3 allows a determination not only of the temperature ( as a ratio of the slopes ) but also of  $\ln(K(T))$  from the comparison of the zero order coefficients ( constants ) using the extracted temperature. The resulting values of  $T$  are given in Fig. 4 for the different quasiprojectile excitation energy bins.

The dependence of the temperature on the excitation energy ( caloric curve ), given in Fig. 4 ( solid squares ), is compared to the experimental caloric curve obtained for the same set of data by the double isotope ratio method for the thermometer  $d,t/^3\text{He},^4\text{He}$  ( dashed line indicates the double isotope ratio temperature and solid lines indicate statistical errors ). The agreement between the two plots is reasonable. Both methods give the value of the temperature between 5 and 7 MeV for the apparent excitation energies above 5 A MeV. The agreement between temperatures determined by the two different methods shows that the assumptions made for  $\mu_n - \mu_p$  reflect the physical trends which take place in the freeze-out configuration. Since the multiplicity of the charged fragments decreases with decreasing  $\epsilon_{app}^*$ , the decrease of the determined temperatures in the lowest bins of  $\epsilon_{app}^*$  may be a signature

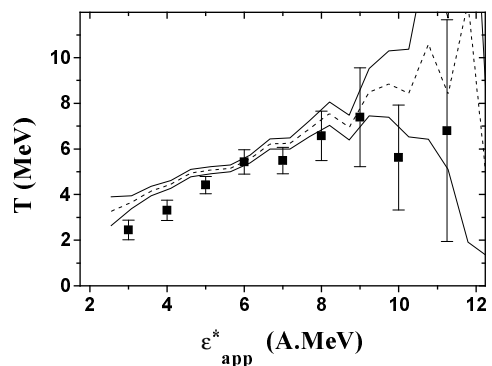


Figure 4. Dependence of the temperature  $T$ , determined from the dependence of the yield ratio  $Y(^3\text{H})/Y(^3\text{He})$  on the N/Z ratio of the quasiprojectile, on  $\epsilon_{app}^*$  ( solid squares )<sup>4</sup>. Dashed and solid lines indicate the values and the statistical deviations of the double isotope ratio thermometer d,t/<sup>3</sup>He,<sup>4</sup>He.

of the onset of a low energy deexcitation mode where several neutrons and light charged particles are emitted prior to the breakup of the partially cooled residue into two massive fragments ( such a mass distribution is observed in the channels with 3 and 4 charged fragments ). The temperatures determined thus become mean values representing the range of temperatures at which hydrogen and helium isotopes are emitted during the deexcitation cascade.

### 3 Isospin asymmetry of reaction products originating from projectile-target systems with different N/Z

With increasing violence of the nucleus-nucleus collision a hot composite system can be created. Such a source can consist of parts of both the projectile and target. The excitation energy of such a source is high enough for emission of intermediate mass fragments ( IMF ). Another possibility for emission of intermediate mass fragments is a dynamical scenario where a neck is formed and IMFs are remnants of its rupture. Information on both mass and charge of emitted IMFs can be crucial for the determination of the emission mechanism and thus properties of the emitting source.

Four reactions of <sup>124</sup>Sn, <sup>124</sup>Xe beams with <sup>112,124</sup>Sn targets have been studied at 28 A MeV<sup>9</sup> at the Cyclotron Institute of Texas A&M University using the 4 $\pi$  multi-detector array NIMROD<sup>10</sup>. The aim of the experiment was to study the interplay of isospin degree of freedom with reaction dynamics

of the projectile-target system. NIMROD is a  $4\pi$  neutron and charged particle detection system. Neutrons are detected using a liquid scintillator which is contained in vessels around the target. Charged particles are detected using 96 charged particle detection modules in 12 rings. A typical detection module consists of a gas ionization chamber and one or two CsI(Tl) detectors. In each ring there are several modules where one or two silicon detectors are placed between the ionization chamber and CsI(Tl) detector. NIMROD has nearly complete coverage for both charged particles and neutrons as well as selective coverage for isotopically resolved charged particles up to oxygen. An isospin asymmetry of the reaction products can be examined with respect to the observables characterizing the dynamical evolution of different projectile-target systems. The systems studied have significantly different values of initial isospin asymmetries of both projectile and target.

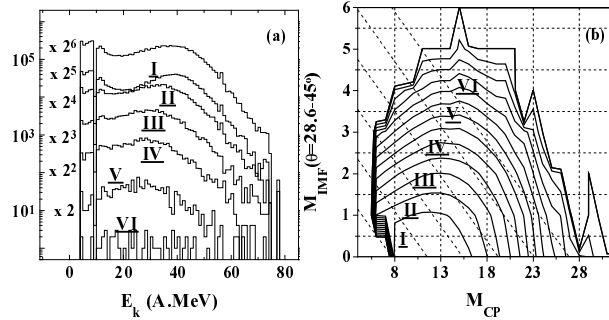


Figure 5. (a) - Inclusive spectrum of  $\alpha$ -particles ( top ) from reaction  $^{124}\text{Xe} + ^{124}\text{Sn}$  and spectra for 6 centrality bins ordered from top to bottom by increasing centrality <sup>9</sup>. (b) - Centrality cuts in the  $M_{IMF}$  vs.  $M_{CP}$  histogram. Skewed lines indicate centrality cuts used in (a), horizontal and vertical lines indicate one-dimensional cuts in  $M_{IMF}$  and  $M_{CP}$  histograms.

Newly developed calibration methods <sup>11</sup> have been employed in data analysis. The calibration coefficients are obtained from a minimization procedure where three isotope lines assigned in the experimental two-dimensional spectra are fitted to the calculated energy losses in the telescope. A functional for dependence of energy on light output in the CsI(Tl) detector was taken from ref. <sup>12</sup>. An example of calibrated  $\alpha$ -spectra <sup>9</sup> with different centralities is shown in Fig. 5a. The spectra were collected at angles  $11.0-14.9^\circ$  in one of the Si-Si-CsI(Tl) telescopes. Both inclusive spectrum ( top one ) and spectra collected in several centrality bins ( centrality increases from top to bottom, multiplication coefficients of spectra differ by factor of two ). Centrality cuts have



been made in the two-dimensional histogram of IMF multiplicities ( $M_{IMF}$ ) vs multiplicities of charged particles ( $M_{CP}$ ) by parallel cuts chosen so that the most central cut selects the events along the line connecting the events with highest multiplicities of charged particles and highest IMF multiplicities ( see Fig. 5b ). Such a selection unifies both criteria and adds events of analogous centrality where the content of IMFs and charged particles is between both extremes. Event shape analysis was carried out and showed analogous trends in terms of sphericity and coplanarity. With increasing centrality the  $M_{IMF}$  criterion selects the values of flow angle still closer to  $90^\circ$ , while  $M_{CP}$  criterion selects still lower flow angles. The unified criterion selects events with slowly changing flow angles between the former two. The statistics in the most central cut increased by two orders of magnitude. Fig. 5a shows that also the shapes of spectra change gradually with increasing centrality.

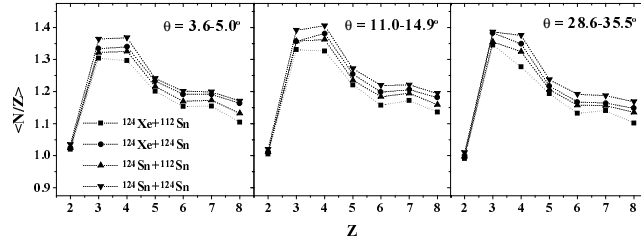


Figure 6. Mean N/Z-ratios of emitted LCPs and IMFs with  $Z=2-8$  from four reactions obtained using the inclusive data from three Si-Si-CsI(Tl) telescopes positioned at different angles <sup>9</sup>.

In Fig. 6 are given the mean N/Z-ratios of emitted LCPs and IMFs with  $Z=2-8$  from four reactions obtained using the inclusive data from three Si-Si-CsI(Tl) telescopes positioned at different angles <sup>9</sup>. The overall dependence is similar at all angle ranges. He-isotopes ( $Z=2$ ) are dominated by  $\alpha$ -particles. Mean N/Z ratios are highest for Li- ( $Z=3$ ) and Be-isotopes ( $Z=4$ ) and decrease gradually with increasing atomic number of IMFs. When comparing mean N/Z ratios from four reactions of  $^{124}\text{Sn}, ^{124}\text{Xe}$  beams with  $^{112}, ^{124}\text{Sn}$  targets two characteristic patterns can be distinguished. At forward angles  $3.6-5.0^\circ$  mean N/Z ratios of Li- and Be-isotopes appear to track with the isospin asymmetry of the whole projectile-target system what creates a typical 1-2-1 pattern. On the other hand the isotopes with  $Z=5-8$  appear to track with the isospin asymmetry of the target nucleus what creates a 2-2 pattern. At angles  $11.0-14.9^\circ$  the 1-2-1 pattern can be identified for Li- and Be-isotopes while for heavier fragments the pattern vary for different

atomic numbers. At angles  $28.6-35.5^\circ$  one can recognize the 2-2 pattern for Li-isotopes while at heavier fragments the 1-2-1 pattern dominates. In principle, one can identify the 1-2-1 pattern to the origin of fragments emitted from hot composite source and 2-2 pattern to the emission from quasiprojectile. The fragments with  $Z=5-8$  at forward angles can be possibly attributed to binary de-excitation channels of the moderately excited quasiprojectile while the 2-2 pattern of Li-isotopes at the most central angle range may suggest either backward emission from the quasiprojectile or emission from quasitarget. Similar isospin asymmetry patterns ( 1-2-1 and 2-2 ) can be observed also in the isotope yield distributions. More detailed studies including also constraints on different centralities are now in progress. In any case the data demonstrates that the isospin asymmetry of emitted fragments is a sensitive probe of the reaction dynamics.

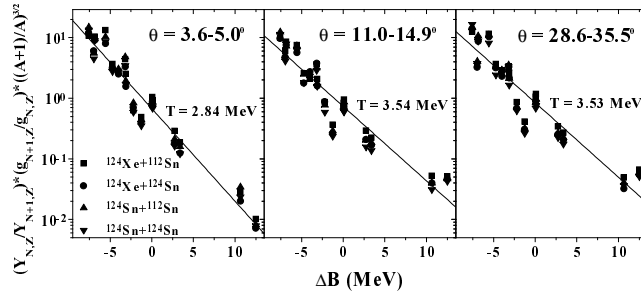


Figure 7. Systematics of corrected isotopic ratios  $Y_{N,Z}/Y_{N+1,Z}$  from four reactions plotted against the difference of binding energies <sup>9</sup>.

Fig. 7 shows the systematics of corrected isotopic ratios  $Y_{N,Z}/Y_{N+1,Z}$  from the four reactions plotted against the difference of binding energies <sup>9</sup>. The inclusive data from the three Si-Si-CsI(Tl) telescopes positioned at different angles was used. Isotopic ratios were corrected to g.s. spin and mass in order to investigate eventually the possibility to estimate the temperature at which fragments have been emitted. For the macrocanonical ensemble the quantity shown in Fig. 7 becomes proportional to  $e^{-\frac{\Delta B}{T}}$  when assuming that the difference of free energies can be approximated by difference of binding energies. The experimental systematics given in Fig. 7 appears to follow a similar trend. There are no significant differences for data from different reactions. Apparent temperature at given angles was estimated using exponential fits to data ( see Fig. 7 ). It is lowest at forward angles and appears to saturate at more central angles. It is one of the goals of further analysis to

obtain similar information for subsets of data with well defined centrality and excitation energy and to carry out comparison to various double isotope ratio thermometers.

#### 4 Production mechanism of the hot source

In order to create a hot source, a considerable part of the kinetic energy should be damped into thermal degrees of freedom. Hot source can be created both in damped peripheral and violent collisions. In damped peripheral collisions projectile and target nuclei preserve their identity and a di-nuclear system is created due to friction forces. In such cases a considerable amount of nucleons can be exchanged what leads to dissipation of a significant part of the available energy into heat. As demonstrated in section 2 the model of deep inelastic transfer combined with an appropriate de-excitation model can reproduce the experimental data very precisely. This will be further demonstrated in the next section. With decrease of the impact parameter the energy of the radial motion increases and violent scenarios can take place where essential parts of both nuclei join into one hot nucleus. A hybrid model for such a collisions was developed by one of us recently <sup>13</sup>. In order to describe the reaction dynamics consistently, pre-equilibrium emission was taken into account phenomenologically. The hot source is created by incomplete fusion of the participant zone with one of the spectators. The other spectator forms a relatively cold source. Motion along classical Coulomb trajectories is assumed. The results of the model calculation were compared to wide range of experimental data and a consistent description was obtained <sup>13</sup>.

The capabilities of the model are illustrated in Fig. 8 where experimental spectra of  $\alpha$ -particles and  ${}^7\text{Li}$ -fragments obtained using the NIMROD detector in the reaction  ${}^{124}\text{Sn}(28\text{A MeV})+{}^{28}\text{Si}$  at three angles <sup>9</sup> are compared to the results of model calculation. The reaction studied is inverse of the reactions studied in section 2 and one can expect that the high energy IMFs emitted at forward angles originate from violent collisions. Nucleon exchange usually leads to the close to equal excitation energy sharing what in mass asymmetric systems leads to the very hot light nucleus while the heavy one remains cold. The excitation energy high enough for emission of IMFs can be concentrated in the hot heavy composite source created in violent collisions. The SMM code <sup>7</sup> was used for the de-excitation of both the hot heavy source and the cold target remnant. No mutual Coulomb interaction of de-exciting sources was assumed in the calculation. The same normalization of the simulated data is used for both fragments and all angle ranges. The model calculation describes the essential features of the experimental spectra at all angles. According to

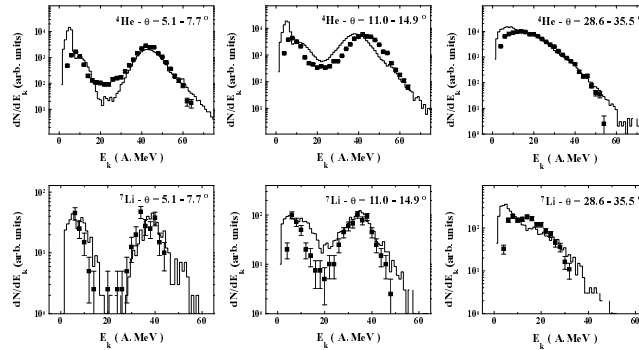


Figure 8. Experimental spectra ( symbols ) of  $\alpha$ -particles and  ${}^7\text{Li}$ -fragments obtained using NIMROD detector in the reaction  ${}^{124}\text{Sn}(28\text{A.MeV})+{}^{28}\text{Si}$  at three angles <sup>9</sup> compared to the results of model calculation ( histograms ).

the calculations the dips in the spectra at forward angles correspond to the velocity of emitting source. The remaining discrepancies can be possibly attributed to the mutual Coulomb interaction between the hot and cold sources which was not taken into account. In order to account for mutual Coulomb interaction between sources an additional assumptions concerning their distance should be introduced. Further investigations focused on this topic are in progress.

## 5 Production of neutron-rich nuclides using ${}^{86}\text{Kr}$ beam at projectile energy 25 A MeV

As already pointed out, peripheral reactions between massive nuclei at the Fermi energy domain involve considerable exchange of nucleons. As a result, rare isotopes ( either proton-rich or neutron-rich ) can be produced with large cross sections. This possibility, in regards to the production of neutron rich nuclides was recently explored in the reaction of neutron-rich  ${}^{86}\text{Kr}$ -beam with a neutron-rich  ${}^{64}\text{Ni}$ -target.

In a recent study <sup>14</sup>, a 25 A MeV  ${}^{86}\text{Kr}^{22+}$  beam from the K500 superconducting cyclotron, with a typical current of  $\sim 1$  pA, interacted with a  ${}^{64}\text{Ni}$  target of thickness  $4 \text{ mg/cm}^2$ . The reaction products were analyzed with the MARS spectrometer <sup>15</sup>. The primary beam struck the target at  $0^\circ$  relative to the optical axis of the spectrometer. The direct beam was collected in a small square Faraday cup ( blocking the angular range  $0-1^\circ$  ), while the

fragments were accepted in the angular range 1.0–2.7°. MARS optics<sup>15</sup> provides one intermediate dispersive image and a final achromatic image ( focal plane ). At the focal plane, the fragments were collected in a large area ( 5×5 cm ) three-element (  $\Delta E_1$ ,  $\Delta E_2$ , E ) Si detector telescope. The  $\Delta E_1$  detector was a position-sensitive Si strip detector of 63  $\mu\text{m}$  thickness whereas the  $\Delta E_2$  and the E detector were single-element Si detectors of 150 and 950  $\mu\text{m}$ , respectively. Time of flight was measured between two PPACs ( parallel plate avalanche counters ) positioned at the dispersive image and at the focal plane, respectively, and separated by a distance of 13.2 m. The PPAC at the dispersive image was also X–Y position sensitive and used to record the position of the reaction products. The horizontal position, along with NMR measurements of the field of the MARS first dipole, was used to determine the magnetic rigidity  $B\rho$  of the particles. Thus the reaction products were characterized by an event-by-event measurement of  $dE/dx$ , E, time of flight, and magnetic rigidity. The response of the spectrometer/detector system to ions of known atomic number Z, mass number A, ionic charge q and velocity was calibrated using low intensity primary beams of  $^{40}\text{Ar}$  and  $^{86}\text{Kr}$  at 25 A MeV.

The determination of the atomic number Z was based on the energy loss of the particles in the first  $\Delta E$  detector and their velocity and is described in more detail in<sup>14</sup>. The Z resolution was 0.5 units ( FWHM ) for near-projectile fragments. The ionic charge  $q$  of the particles entering MARS was obtained from the total energy  $E_{tot}=\Delta E_1+\Delta E_2+E$ , the velocity and the magnetic rigidity according to the expression:

$$q = \frac{3.107}{931.5} \frac{E_{tot}}{B\rho(\gamma - 1)} \beta\gamma \quad (4)$$

where  $E_{tot}$  is in MeV,  $B\rho$  in Tm,  $\beta = v/c$  and  $\gamma = 1/(1 - \beta^2)^{\frac{1}{2}}$ . The measurement of the ionic charge  $q$  had a resolution of 0.4 units ( FWHM ). Since the ionic charge must be an integer, we assigned integer values of  $q$  for each event by putting windows (  $\Delta q = 0.4$  ) on each peak of the  $q$  spectrum. Using the magnetic rigidity and velocity measurement, the mass-to-charge  $A/q$  ratio of each ion was obtained from the expression:

$$A/q = \frac{B\rho}{3.107\beta\gamma} \quad (5)$$

Now, combining the  $q$  determination with the  $A/q$  measurement, the mass A was obtained as:

$$A = q_{int} \times A/q \quad (6)$$

(  $q_{int}$  is the integer ionic charge determined as above ) with an overall resolution ( FWHM ) of about 0.6 A unit ( See Fig. 9 ).

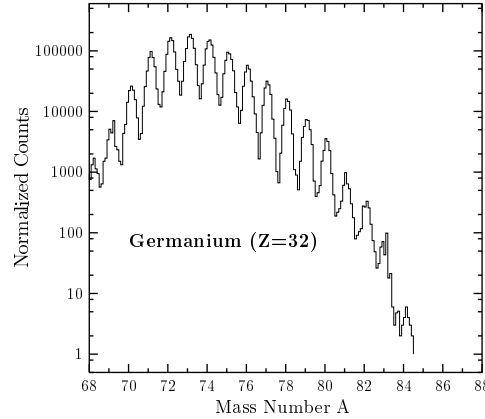


Figure 9. Mass histogram of Germanium (Z=32) isotopes <sup>14</sup>.

Combination and normalization of the data at the various magnetic rigidity settings of the spectrometer, and summation over all ionic charge states ( with corrections applied for missing charge states ), provided fragment distributions with respect to Z, A and velocity. Fig. 9 shows the mass spectrum of Z=32 isotopes in full resolution. Results on the mass distributions ( cross sections ) of several elements are shown in Fig. 10 ( solid points ) and are compared to reaction simulations appropriate for this energy regime.

The simulations of the present reaction involve the deep inelastic transfer code of Tassan-Got <sup>6</sup> for the primary interaction stage. Following the creation of the primary fragments, the statistical de-excitation of the excited primary fragments was simulated using the code GEMINI <sup>16</sup>. Each partial wave distribution was appropriately weighted and combined to give the overall fragment Z, A ( and velocity ) distributions. In Fig. 10, the mass distributions for elements Z=30–35, calculated by this model, are shown as open squares. The heavy dashed lines are predictions of the EPAX parametrization <sup>17</sup> of relativistic fragmentation cross sections and is plotted here for comparison. ( Note that, in high-energy fragmentation, nucleon-pickup products are not produced—or, at best, are highly suppressed compared to lower energy peripheral collisions ). As we see in Fig. 10, neutron-rich nuclides are produced in substantial yields. For near projectile elements, an enhancement in the production is observed that can not be described by the simulations. This

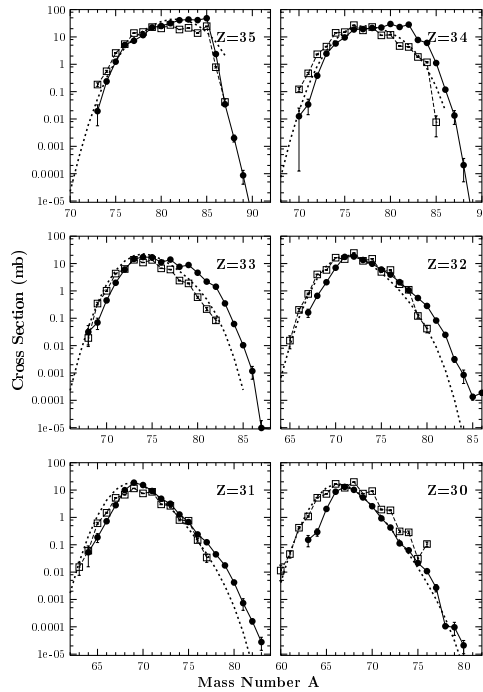


Figure 10. Mass distributions of several elements from the reaction of 25 A MeV  $^{86}\text{Kr}$  with  $^{64}\text{Ni}^{14}$ . The present data are shown by full symbols. Open symbols are simulations according to DIT/GEMINI and the dashed line is from the high-energy parametrization EPAX ( see text ).

enhancement takes place at masses close to the beam and thus in the very peripheral reactions where the nucleon exchange can be restricted to neutron-rich surface region of the target nucleus. Further investigation of this finding is currently underway.

In Fig. 11, the gross features of the distributions are described. In Fig. 11a, the mass yield curve is presented. The measured data are given as open symbols. The result of the DIT/GEMINI calculation, filtered by the spectrometer angular and momentum acceptance is given by the dashed line, whereas the full line gives the total ( unfiltered ) yield. Using the ratio of filtered to unfiltered calculated yield, correction factors for the acceptance of the spectrometer were obtained as a function of mass and were applied to the measured yield data to obtain the total yield, given by the full symbols in the figure.

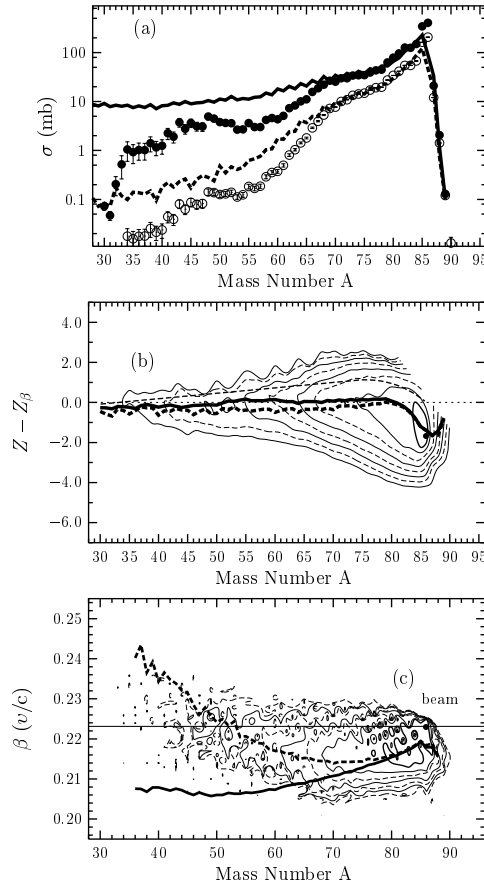


Figure 11. Fragment distributions for the reaction of 25 A MeV  $^{86}\text{Kr}$  with  $^{64}\text{Ni}^{14}$ . (a) - isobaric yield distribution. The data are shown as solid points. The full line is the result of DIT/GEMINI ( see text ). The dashed line is the result of the same calculation as the full line, but with a cut corresponding to the angular and momentum acceptance of the spectrometer. (b) - yield distributions as a function of  $Z$  ( relative to the line of  $\beta$  stability,  $Z_\beta$  ) and  $A$ . Highest yield contours are plotted with thicker lines. Successive contours correspond to a decrease of the yield by a factor of 2. The calculated values from DIT/GEMINI are shown as i) thick full line: without acceptance cut and, ii) thick dashed line: with acceptance cut. Thin dashed line: EPAX parametrization. (c) - velocity vs. mass distributions. Data are shown as contours as in (b). The thick lines are as in (b). The horizontal full line represents the beam velocity.



These correction factors were also employed to obtain total isotope production cross sections ( as e.g. given in Fig. 10 ) from the measured yields. In Fig. 11b, the measured yield distributions as a function of  $Z$  ( relative to the line of  $\beta$  stability,  $Z_\beta$  ) and  $A$  are presented as contour lines. The calculated values from DIT/GEMINI are shown as thick full line ( without acceptance cut ) and as a thick dashed line ( with acceptance cut ). The thin dashed line is from the EPAX parametrization<sup>17</sup>. Finally, in Fig. 11c, the velocity vs. mass distributions are given. The present data are shown as contours as in Fig. 11b. The thick full line is from the DIT/GEMINI calculation without acceptance cut and the dashed line is with acceptance cut. In general, we see that the DIT/GEMINI calculations are able to provide a satisfactory quantitative description of the observed gross distributions. Also, it does a fair job in predicting the absolute values of the production cross sections ( except for the very n-rich isotopes, as already pointed out ).

From a practical standpoint, using the present cross section results we can make estimates of rare beam rates from intense beams at this energy regime. Assuming a beam of 100 pA  $^{86}\text{Kr}$  at 25 A MeV striking a 10 mg/cm<sup>2</sup>  $^{64}\text{Ni}$  target, we give two indicative rate estimates for rare beams: First, for  $^{84}\text{Se}$  ( two-proton removal product, cross section 6 mb ) the rate is  $\sim 3.6 \times 10^5$  particles/s. Second, for the more exotic  $^{87}\text{Se}$  ( two-proton removal+three-neutron pickup product, cross section  $\sim 12\mu\text{b}$  ) the rate is about 800 particles/s. Such yields of rare isotopes may enable a variety of nuclear structure and nuclear reaction studies in the Fermi energy regime.

In general, from the present experimental study and calculations, we see that such reactions, near the Fermi energy, involving extensive nucleon exchange between the projectile and the target, can be utilized as an efficient way to produce very neutron-rich nuclei. Apart from in-flight possibilities, the option of exploiting this type of reaction ( in normal or inverse kinematics ) at these ( or lower ) energies for rare isotope production in an IGISOL-type concept is currently under way at Texas A&M.

## 6 Conclusions and outlook

As shown in previous sections, detailed studies of nucleus-nucleus collisions in the Fermi energy domain can provide deep insight into multifragmentation phenomena. Of special interest are further detailed studies of the isospin asymmetry of the emitted fragments which appears to be a sensitive probe into the reaction dynamics. From a practical point of view, the Fermi energy domain offers unique possibilities for production of neutron-rich rare nuclides. The ways to utilize such possibilities will be explored in the near future.

## Acknowledgments

This work was supported in part by the Robert A. Welch Foundation through grant No. A-1266 and the Department of Energy through grant No. DE-FG03-93ER40773. M. V. was partially supported through grant VEGA-2/1132/21.

## References

1. R. Laforest *et al.*, *Phys. Rev. C* **59** (1999) 2567.
2. M. Veselsky *et al.*, *Phys. Rev. C* **62** (2000) 064613.
3. M. Veselsky *et al.*, *Phys. Rev. C* **62** (2000) 41605(R).
4. M. Veselsky *et al.*, *Phys. Lett. B* **497** (2001) 1.
5. F. Gimeno-Nogues *et al.*, *Nucl. Inst. and Meth. A* **399** (1997) 94.
6. L. Tassan-Got, C. Stéfan, *Nucl. Phys. A* **524** (1991) 121.
7. J.P. Bondorf *et al.*, *Phys. Rep.* **257** (1995) 133.
8. G. Audi, A.H. Wapstra, *Nucl. Phys. A* **595** (1995) 409.
9. NIMROD Collaboration: M. Veselsky *et al.*, in preparation.
10. N. Marie *et al.*, Progress in Research, 1997–1998, Cyclotron Institute, Texas A&M University, p. V-19; R. Wada *et al.*, Progress in Research, 1998–1999, Cyclotron Institute, Texas A&M University, p. V-15.
11. M. Veselsky *et al.*, in preparation,  
see also [http://cyclotron.tamu.edu/progress/2000-2001/5\\_a13.pdf](http://cyclotron.tamu.edu/progress/2000-2001/5_a13.pdf).
12. L. Tassan-Got, nucl-ex/0103004.
13. M. Veselsky, nucl-th/0107062.
14. G.A. Souliotis *et al.*, in preparation.
15. R.E. Tribble *et al.*, *Nucl. Instr. and Meth. A* **285** (1989) 441.
16. R. Charity *et al.*, *Nucl. Phys. A* **483**(1988) 391.
17. K. Sümmerer, B. Blank, *Phys. Rev. C* **61** (2000) 034607.